Feedbacks Between Magmatic Intrusions, Faulting, and Surface Processes at Continental Rifts

Thomas A. Morrow[1]*, Jean-Arthur Olive[2], Mark Behn[1], Paris Smalls[3]

* corresponding author: thomas.morrow@bc.edu 1. Boston College, Chestnut Hill, MA 2. École Normale Supérieure, Paris, France

3. Joint Program in Oceanography/Applied Ocean Science and Engineering, Massachusetts Institute of Technology/Woods Hole Oceanographic Institution, Woods Hole, MA

Abstract

During continental rifting, faulting, magmatic injection, and surface processes collectively shape the landscape. Although feedbacks between surface processes and faulting at rifts have been explored, the relationship between shallow magmatic intrusions, topography, and surface processes is poorly understood. Magmatic injection is controlled in part by lithospheric stress, and should therefore respond to rift-associated perturbations to the stress field. Along with normal fault formation and evolution, surficial mass redistribution via erosion, sediment transport, and deposition alters lithospheric stresses and has the potential to influence dike emplacement and long-term rift structure.

Here we present a series of two-dimensional (2–D) numerical model runs utilizing the particle-in-cell, finite difference code SiStER to quantify the feedbacks between tectonic, magmatic, and surface processes that shape continental rifts. In our models, extension is accommodated through a combination of magmatic intrusion and tectonic stretching. Magmatic intrusion occurs within a narrow region when and where the sum of horizontal deviatoric stress and magmatic overpressure exceeds the tensile strength of the lithosphere. Magmatic overpressure is thus a key parameter that strongly modulates the sensitivity of dike emplacement to faulting, bending, and topographically-induced variations in lithosphere stress.

Our results first probe the relationships between fault-related stresses and the timing and depth-distribution of magmatic intrusions at a rift with no active surface processes. In these cases, the locus of magmatic spreading migrates vertically in response to the evolving stress field. The 2–D tectonic model is then coupled to a 1–D landscape evolution model, which modifies topography concurrent with extension. In the simplest case, topographic diffusion effectively redistributes the topographic load, contributing to variations in injection-controlling lithospheric stresses. We compare our tectonic-responsive results with models that incorporate active surface processes to constrain the conditions under which surface processes modulate magmatic injection. **Our simulations suggest that the development and redistribution of topography exerts an important control on the partitioning of tectonic and magmatic strain at extensional plate boundaries.**

Motivation

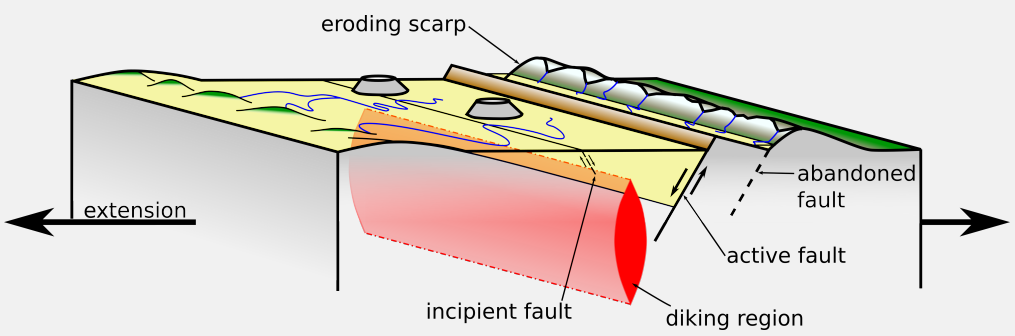

Figure 1: Conceptual model At continental rifts, extension is accommodated by faulting and magmatic intrusion (diking). During rift evolution, erosion and sedimentation continually alter the landscape, influencing the stress state of the lithosphere, the life-span of normal faults, and regions where along-rift dike propagation may or may not be favorable.

- During rifting, erosion and deposition modulate landscape evolution as well as fault growth and lifespan.
- Dike injection and magmatic accommodation of extension are sensitive to variations in lithospheric stress.
- Surface processes and fault growth modulate the stress state of the lithosphere and thus control regions where dike injection is favorable.

How do feedbacks between fault growth, rift topography, surface processes, and magmatic injection work to shape rift evolution?

Numerical methods

Tectonic Model

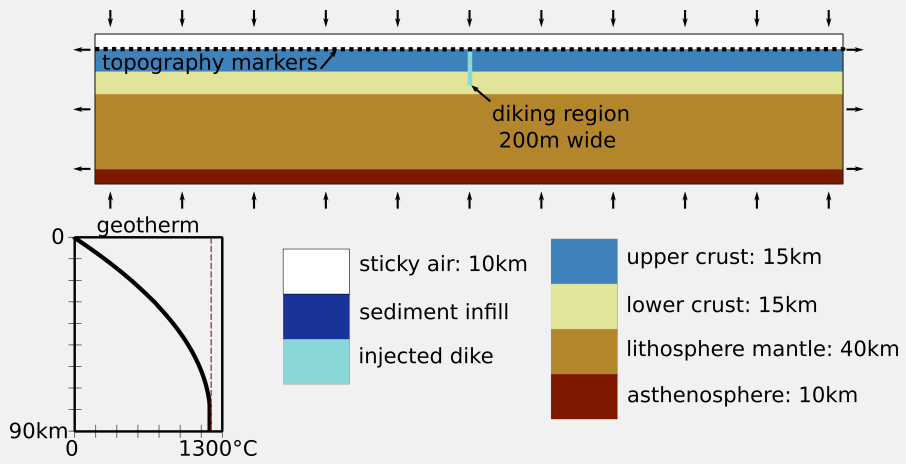

Figure 2: Model domain, boundary, rheology, and initial conditions

The numerical code **SiStER** [*Olive et al.,* 2016] solves for the conservation of mass(1), momentum(2), and energy(3) using a finite-differencing scheme on a fully staggered grid. In equations (1–2), v indicates velocity, σ'_{ij} denotes deviatoric stress (indices i and j indicate the vertical or horizontal direction respectively; repeated indices indicate summation), and T is temperature. Density, heat capacity, and thermal conductivity are ρ, c_p, and k, respectively. The right-hand side of equation 1 accounts for regions where dike injection occurs, where M is the fraction of magmatically accommodated extension, $U_{1/2}$ is half the extension rate, and dx is the dike injection width. In equation 3, $\frac{DT}{Dt}$ is the material time-derivative of T.

$$\frac{\partial v_i}{\partial x_i} = \begin{cases} \frac{2MU_{1/2}}{dx}, & \text{in injection region} \\ 0, & \text{otherwise} \end{cases} \quad (1)$$

$$\frac{\partial \sigma_{ij}}{\partial x_j} - \frac{\partial P}{\partial x_i} + \rho g_i = 0, \quad (2)$$

$$\rho C_p \frac{DT}{Dt} = \frac{\partial}{\partial x_i}\left(k \frac{\partial T}{\partial x_i}\right) + H, \quad (3)$$

The model domain is 500 km x 100 km with a maximum resolution of 500 m and comprised of five layers. A "sticky air" layer at the top of the domain allows for free surface behavior. The lithosphere is comprised of two layers overlying lithospheric mantle. The base of the model is asthenospheric mantle. Compensating inflow from the top and bottom balance mass outflow from the model sides. The sides of the domain are insulating and the base of the model is fixed at 1300°C. Material properties are tracked and advected using a marker-in-cell scheme. Rheologic and material parameters are listed in 2.

We implement a visco-elastic-plastic rheology, assuming that the lithosphere behaves as a Maxwell solid; history terms for stored elastic stresses are added to the right side of equation 2. Plastic deformation occurs when stresses surpass the brittle yield stress determined by a Drucker-Prager failure criterion, producing localized shear bands that behave similar to faults. At greater temperatures, deeper mantle material deforms viscously.

Magmatic Accommodation of Extension

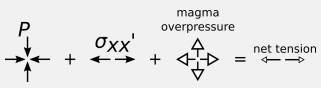

Figure 3: Dike injection occurs when the combination of pressure, deviatoric stress, and magmatic overpressure yields a net tensile condition.

A region of diking and magmatically-accommodated extension is simulated following the approach of *Lavier* [2000] and *Behn and Ito* [2008]. When an injection node is in a net tensile condition, a source mass term corresponding to the magmatic fraction of extension produced and proportionate to the tensile stress in the diking region, M, is added to the right hand side of equation 1. A source term in the right hand side of equation 3 accounts for heat due to intrusion and latent heat of crystallization in the dike.

Landscape Evolution Model

The tectonic model is coupled to a landscape evolution model [*Braun & Willet, 2012*] that instantaneously infills sediment to a pre-defined depth and erodes uplifted landscape via stream power incision and hillslope diffusion

$$\frac{\partial z}{\partial t} = U - KA^m S^n + D\nabla^2 z \quad (4)$$

where U is tectonic uplift, K is erodibility, A is drainage area, S is local slope, m and n are constants, and D is hillslope diffusivity [e.g., *Anderson & Anderson,* 2010]. Sedimentation and infill is turned off for case 3 below.

Code structure

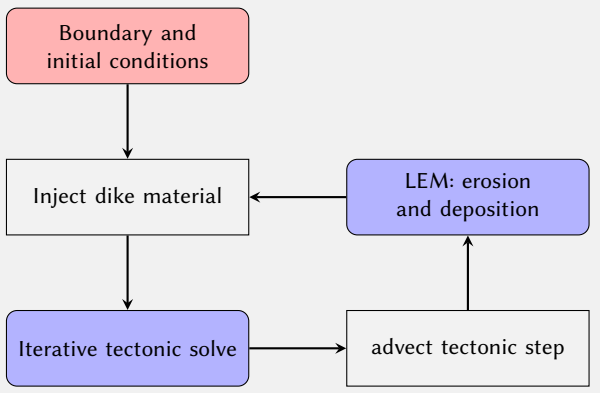

The numerical code progresses by determining the locations where dike injection is favorable, adding mass source terms to the right hand side of equation 1, and then iteratively solving. After a solve, material markers advect following the velocity solution over a tectonic timestep. Then, the topographic surface generated by the tectonic solve is passed to the landscape evolution model. Over a number of landscape solve timesteps whose sum equals the total tectonic timestep, the landscape is modified following equation 4. Topography markers are modified in the tectonic model to mimic the mean landscape profile and "sticky air" markers below the sedimentation level are converted to a sediment phase. Dike-controlling stresses and pressures are updated, new material is injected and the next tectonic solve initiates. Thus, landscape, tectonic, and magmatic features co-evolve and respond to coupled feedbacks.

Results

Here we summarize the long-term feedbacks between dike injection, landscape evolution, and rift development. Additional representative solutions are shown on page 2.

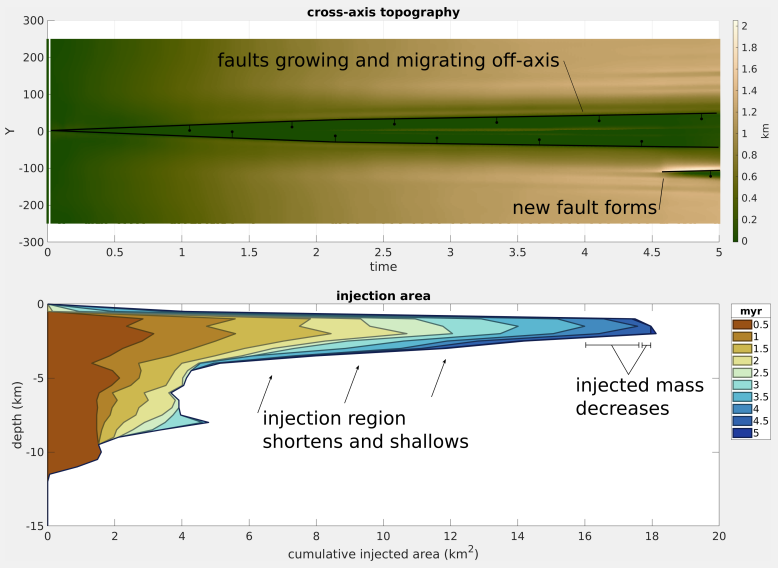

Figure 4: Temporal evolution of cross-axis topography and cumulative dike injection area.

Conclusions

- Magmatic accommodation of spreading migrates vertically during rift evolution and focuses at shallow depths (< 5 km) within 2 myr.
- Injection responds to new fault formation, shutting off when new faults form outward of the rift center (5 myr).
- Less efficient surface processes (lower erodibility) lead to smaller total injection volumes during early rift evolution, likely a result of dike shutoff due to topographic growth.

Feedbacks Between Magmatic Intrusions, Faulting, and Surface Processes at Continental Rifts

Thomas A. Morrow[1]*, Jean-Arthur Olive[2], Mark Behn[1], Paris Smalls[3]

* corresponding author: thomas.morrow@bc.edu 1. Boston College, Chestnut Hill, MA 2. École Normale Supérieure, Paris, France

3. Joint Program in Oceanography/Applied Ocean Science and Engineering, Massachusetts Institute of Technology/Woods Hole Oceanographic Institution, Woods Hole, MA

Model Parameters

Table 1: Model parameters.

Parameter	Notation	Value (units)
Domain size		500 x 100 km
Gravitational acceleration	g	9.8 m s^{-2}
Extension half rate	$U_{1/2}$	1 cm yr^{-1}
Shear modulus	G	30 GPa
Thermal conductivity	k	3.0 W m^{-1} K^{-1}
Heat capacity	C_p	1000 kg m^2 K^{-1} s^{-2}
Coefficient of thermal expansion	α	1x10^{-5} K^{-1}
Heat source terms	H	
Gas constant	R	8.314 J mol^{-1} K^{-1}
Coefficient of friction	μ	0.56
Cohesion	C_0	44 MPa
Critical diking tension	M_0	50–200 MPa
Erodibility	K	1x10^{-4}–1x10^{-6} yr^{-1}
Hillslope diffusivity	D	1x10^{-9} m^2 s^{-1}
Exponential constants	m, n	0.5, 1

Table 2: Rheologic parameters

Parameter	Upper/Lower crust	Injected material	Lithospheric (dry) mantle	Asthenospheric (wet) mantle
Dislocation creep				
Pre-exponential log_{10} Pa^{-n} s^{-1}	-28.0	-21.05	-15.96	-15.81
Exponent	4	4.2	3.5	3.5
Activation energy kj mol^{-1}	223	445	530	480
Activation volume 10^{-6} m^3 mol^{-1}	0	0	13	10
Diffusion creep				
Pre-exponential log_{10} Pa s^{-1}	-	-	-8.16	-8.64
Exponent	-	-	1.0	1.0
Activation energy kj mol^{-1}	-	-	375	335
Activation volume 10^{-6} m^3 mol^{-1}	-	-	6	4

Representative Results

Table 3: Representative results - M_0=50 MPa

inefficient surface processes (erodibility 1x10^{-6} yr^{-1})	efficient surface processes (erodibility 1x10^{-4} yr^{-1})	inefficient surface processes (erodibility 1x10^{-6} yr^{-1}) no sedimentation

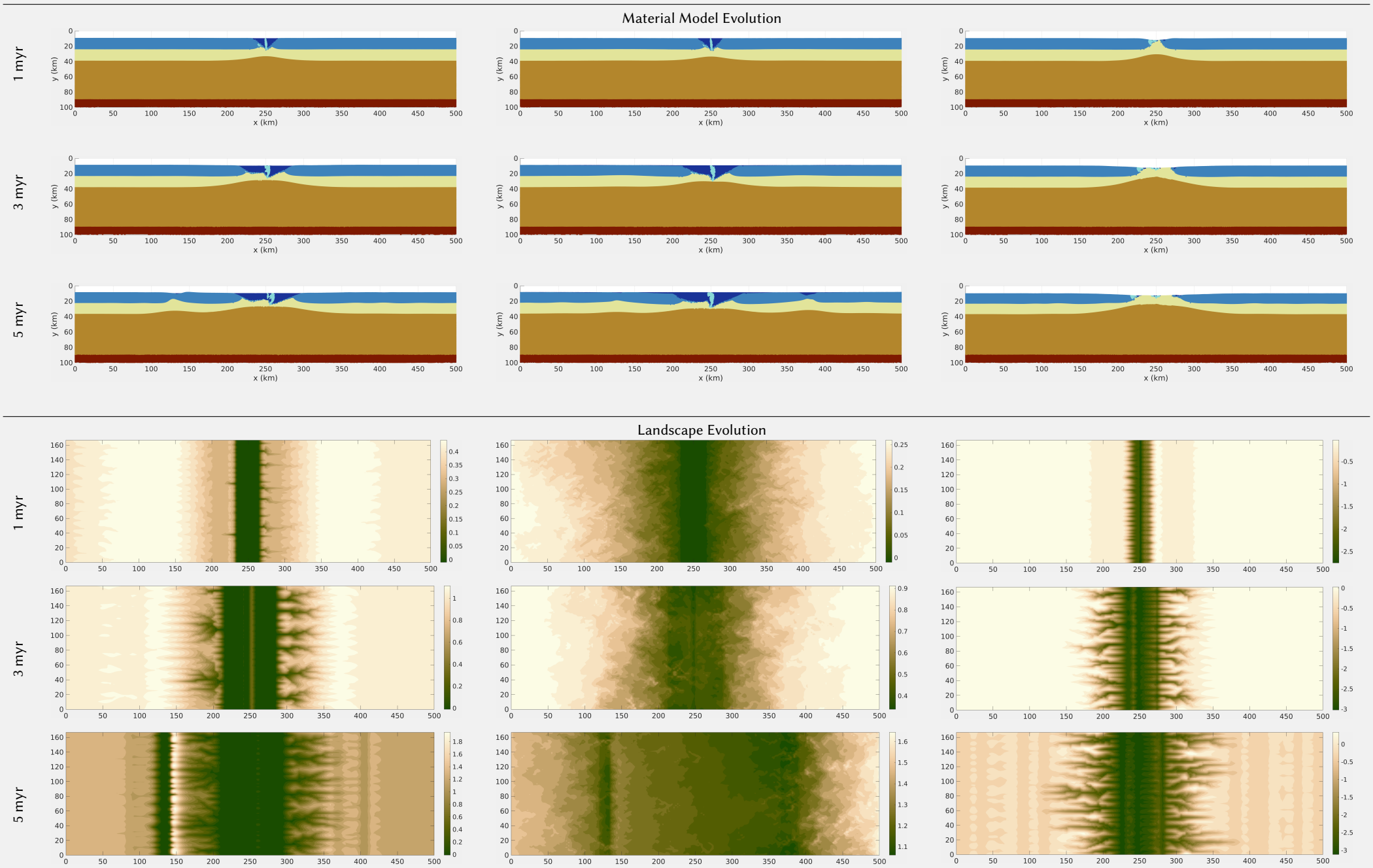

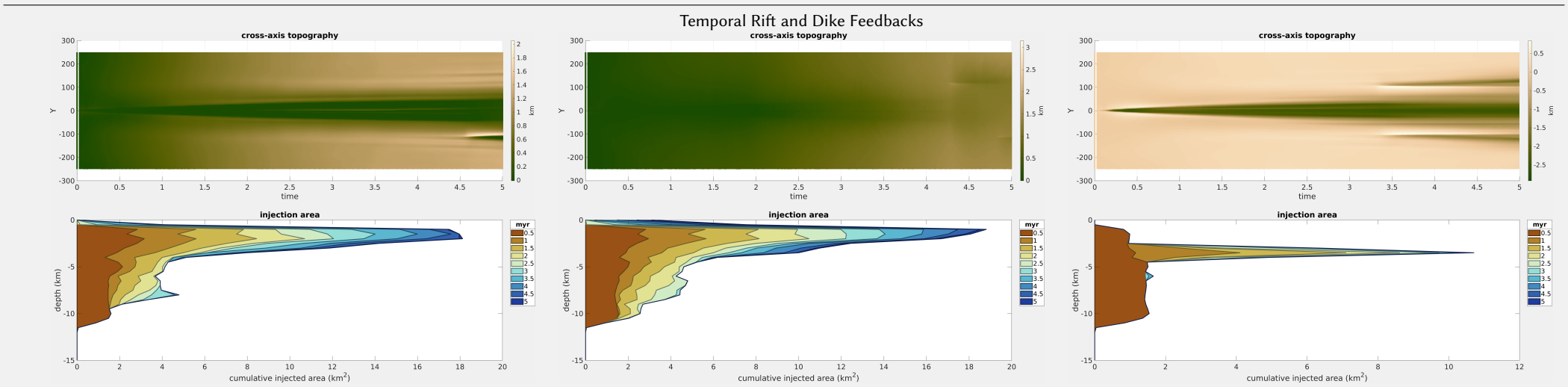

EGU General Assembly 2020

BOSTON COLLEGE

ENS

MIT-WHOI

CC BY